Structure and mobility of water confined in $AlPO_4$-54 nanotubes

Cristina Gavazzoni, Nicolas Giovambattista, Paulo A. Netz, and Marcia C. Barbosa

Citation: The Journal of Chemical Physics **146**, 234509 (2017); doi: 10.1063/1.4985626
View online: https://doi.org/10.1063/1.4985626
View Table of Contents: http://aip.scitation.org/toc/jcp/146/23
Published by the American Institute of Physics

Structure and mobility of water confined in $AlPO_4$-54 nanotubes

Cristina Gavazzoni,[1,a)] Nicolas Giovambattista,[2,b)] Paulo A. Netz,[3,c)] and Marcia C. Barbosa[1,d)]

[1]*Instituto de Física, Universidade Federal do Rio Grande do Sul, Caixa Postal 15051, CEP 91501-970 Porto Alegre, Rio Grande do Sul, Brazil*
[2]*Brooklyn College, City University of New York, 365 Fifth Avenue, New York, New York 10016, USA*
[3]*Instituto de Química, Universidade Federal do Rio Grande do Sul, CEP 91501-970 Porto Alegre, Rio Grande do Sul, Brazil*

(Received 16 March 2017; accepted 26 May 2017; published online 20 June 2017)

We performed molecular dynamics simulations of water confined within $AlPO_4$-54 nanotubes. $AlPO_4$-54 is an artificial material made of AlO_4 and of PO_4 in tetrahedra arranged in a periodic structure forming pores of approximately 1.3 nm in diameter. This makes $AlPO_4$-54 an excellent candidate for practical applications, such as for water filtration and desalination. In this work, the structural and dynamical properties of the confined water are analyzed for various temperatures and water loadings. We find that the water structure is controlled by the heterogeneity of the nanopore surface with the water molecules located preferentially next to the surface of oxygens of $AlPO_4$-54; consequently, at very low densities, water forms helicoidal structures in string-like arrangements. *Published by AIP Publishing.* [http://dx.doi.org/10.1063/1.4985626]

I. INTRODUCTION

Aluminophosphates, $AlPO_4$-*n*, are the first family of framework oxide molecular sieves synthesized without silica.[1] They have periodic structures with pores of nanoscale dimensions, as found in zeolites, and can be prepared in a highly crystalline form.[2] Among all the aluminophosphates, $AlPO_4$-54 is particularly important since it has the largest pores, ≈1.3 nm in diameter. $AlPO_4$-54 possesses unidirectional channels parallel to the *z*-axis formed by 18 AlO_4 and PO_4 tetrahedra with all Al and P cations in 4-fold coordination.[3,4]

Our motivation to study water confined within $AlPO_4$-54 nanotubes is due to the potential application of this material as nanosieve for water treatment. Specifically, the size of the $AlPO_4$-54 pores is large enough to allow for the flow of water molecules, while small enough to filter small organic molecules. In addition, it has been recently acknowledged that water confined in nanoscale pores can flow orders of magnitude faster than the hydrodynamic equations predict.[5–8] This superflow can be explained by the particular arrangements of water molecules in nanoscale confined geometries; for example, water molecules confined within carbon nanotubes can arrange in a single line along the carbon nanotube axis.[5,9–12] The superflow regime of water has been observed mainly in hydrophobic confinement such as carbon nanotubes with diameters in the sub 2-nm scale.[8,13] These studies suggest that in order to enhance the water flow in nanosieves, e.g., for desalination processes,[14] all the nanotubes at the nanosieve have to be sub-2 nm and monodisperse, which is quite a challenge.

Although the chemistry of the confining surface is expected to play a relevant role in the dynamics of water, the surface effects on water dynamics are not well understood. Hydrophilic nanotubes, such as alumina, have been tested for the presence of the superflow. Unfortunately the flow, even though being larger than the expected from theoretical calculations, is much smaller for hydrophilic materials than for the case of carbon nanotubes.[15] An alternative, therefore, is to look for a material that can be easily produced in fixed sizes and that exhibits hydrophobic regions as the carbon nanotubes. This is the case of $AlPO_4$-*n*. Its main advantage over other materials, such as carbon tubes, is that aluminophosphates can be prepared in monodisperse crystalline structures, whereas it is not simple to prepare carbon nanotubes with a precisely controlled diameter. Since $AlPO_4$-*n* has both hydrophobic and hydrophilic groups, it is expected that water flow would be larger for $AlPO_4$-*n* than the flux observed in pure alumina pores. In resume, the $AlPO_4$-*n* tubes are good candidates for water filtration and purification.

Compared to the case of the carbon or the alumina nanotubes, the knowledge of water behavior within $AlPO_4$-54 nanotubes is rather poor. Contrary to the case of carbon and alumina nanotubes, the surface of the $AlPO_4$-54 pore is not atomically smooth, and the high valence of the Al atoms in the $AlPO_4$-54 surface may lead to an irregular distribution of water near the wall. The $AlPO_4$-54 nanopore can exhibit an unusual structural behavior similar to that observed for MoS_2,[16] which shows different water concentrations in the vicinity of Mo or S.

Nanoscale confinement creates a number of effects not observed in the bulk water and such effects can be very sensitive to the properties of the confining surface. For example, confinement can induce the formation of layers,[17–22] the existence of structured phases at the contact layer,[11,12,23] and the

[a)]Electronic mail: crisgava@gmail.com
[b)]Electronic mail: ngiovambattista@brooklyn.cuny.edu
[c)]Electronic mail: netz@iq.ufrgs.br
[d)]Electronic addresses: marcia.barbosa@ufrgs.br and crisgava@gmail.com

shift of the melting temperature to lower values.[24–28] In some cases, water at the solid interfaces can remain liquid-like even for temperatures much below the melting temperature of the bulk water.[26,29] The region in the pressure-temperature phase diagram in which these effects occur depends on the confining geometry,[26,27,30,31] on the dimensions,[32,33] and on the type of water-wall interaction.[16]

In this paper, we study the structural and dynamical properties of the water confined in $AlPO_4$-54 nanopores. Our results are compared with the recent experiments of Alabarse *et al.*[34] This paper is organized as follows. First, we present the computer simulation details and definitions, and we describe the $AlPO_4$-54 structure. In Sec. III, the results are shown and the conclusions are presented in Sec. IV.

II. COMPUTER SIMULATION DETAILS

Molecular dynamics simulations are employed to analyze the behavior of the water confined in the nanotubes of $AlPO_4$-54.[34] We use the TIP4P/2005 water model[35] which reproduces remarkably well many of the properties of bulk water[36] including the diffusivity of the liquid water and the phase diagram of the ice. We consider a full-atomistic model of $AlPO_4$-54. The interactions between water molecules and the pore atoms are modeled by Lennard-Jones and Coulomb pair interaction potentials,

$$V_{ij} = V_{LJ}(r_{ij}) + V_c(r_{ij}) = 4\epsilon_{ij}\left(\left(\frac{\sigma_{ij}}{r_{ij}}\right)^{12} - \left(\frac{\sigma_{ij}}{r_{ij}}\right)^{6}\right) + f\frac{q_i q_j}{\varepsilon_r r_{ij}}, \tag{1}$$

where r_{ij} is the distance between particles, $f = 1/4\pi\varepsilon_0$, and q_i and q_j are the charges of the atoms i and j, respectively. The Lennard-Jones parameters ϵ_{ij} and σ_{ij} are determined by the Lorentz-Berthelot combination rules

$$\sigma_{ij} = \frac{1}{2}(\sigma_i + \sigma_j),$$
$$\epsilon_{ij} = \sqrt{\epsilon_i \epsilon_j}, \tag{2}$$

where σ_i, σ_j, ϵ_i, and ϵ_j are the Lennard-Jones parameters of atoms i and j.

To model $AlPO_4$-54, we use the location of the atoms in the unit cell reported by Alabarse *et al.*,[34] based on X-ray diffraction experiments. We use the Lennard-Jones parameters and partial charges for Al, P, and O proposed by Koh *et al.*[37] and shown in Table I. Since the vibrational motion of the Al, P, and O atoms with temperature is very small, we fix the position of the atoms in $AlPO_4$-54 through the whole simulation run.

TABLE I. Parameters for the $AlPO_4$-54 framework.

	σ(Å)	$\epsilon/k_B(K)$	q (e)
Al	4.008	254.151	+1.4
P	3.695	153.497	+3.4
O	3.118	30.196	−1.2

The simulation box is composed of three unit cells along the x and y directions, and 10 unit cells along the z-axis. Figures 1(a) and 1(b) show the x-y and z-y projections of the system studied. Our system consists of nine pores which allow us to improve the statistics of the water properties studied. In order to visualize the atomic arrangement of the pores' inner surface, we also include in Fig. 1(c) the inner view of a pore.

We perform MD simulations at three temperatures, T = 173, 235, and 293 K. In order to reproduce absorption experiments under different vapor pressures, we perform MD simulations for nine different water loadings, N = 50, 60, 75, 100, 120, 180, 200, 240, and 299.

In order to prepare the systems for a given N, we take a previously equilibrated configuration and include all water molecules in our $AlPO_4$−54 porous system (Fig. 1) which do not overlap with the matrix atoms. Specifically, we remove all water molecules for which the oxygen atom is within a distance d from any atom j of the $AlPO_4$-54 matrix; we define $d = \sigma_O + \sigma_j$, where σ_O is the Lennard-Jones parameter for the water. Molecules within the pores are removed randomly until the desired number of molecules remains in the pore. With this procedure, we are able to fit up to a maximum of N = 299 water molecules in a pore. All simulations are thermalized for t_t = 2 ns followed by a simulation time Δt for data analysis; Δt = 40, 20, and 2 ns for T = 173 K, 235 K, and 293 K, respectively.

Computer simulations are performed using the GROMACS4.6.5[38–40] software package at constant N, T, and V. The temperature is controlled using a Nosé-Hoover

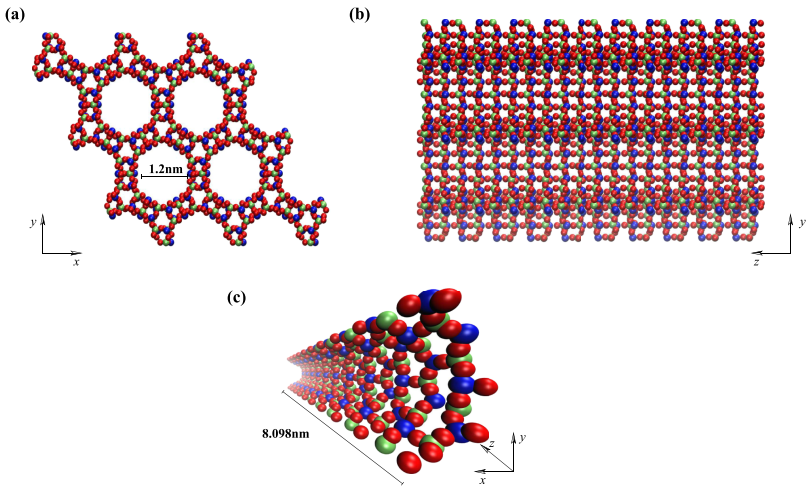

FIG. 1. (a) x-y projection and (b) z-y projection of the $AlPO_4$-54 nanotubes and (c) the inside view of a single nanotube. Red, blue, and green spheres represent, respectively, the oxygen, aluminum, and phosphorus atoms. A single nanotube has the approximated diameter of d = 1.2 nm, and the length of the simulated nanotube is z = 8.098 nm.

thermostat.[41] Water molecule angles and OH bond lengths are maintained constant by using the LINCS algorithm.[42]

We characterize the structure of water within the $AlPO_4$-54 nanopores by calculating the radial density profiles, density colormaps, number of water-water and water-surface hydrogen bonds (HBs), and visual inspection of configurations. Radial density profiles $\rho(r)$ are obtained by calculating the water density inside thin cylindrical shells located at a distance r from the center of the nanotube of radii r and $r + dr$ where $dr = 0.01$ nm.

We consider two kinds of density maps, $x-y$ and $z-\theta$. The $x-y$ colormap is the density map, $\rho(x, y)$, of water molecules projected on the x-y plane. To obtain the $x-y$ colormap, we divide the x-y plane in small bins, between x and $x + dx$ and y and $y + dy$, with $dx = dy = 0.1$ and count the number of water molecules within this bin. Similarly, the $z-\theta$ colormap is the density map, $\rho(z, \theta)$, of water molecules projected on the z-θ plane and is obtained by using the same method used for the $x-y$ colormap. In order to analyze the number of the hydrogen bonds per water molecule, we consider a geometrical definition of HB. Specifically, a water molecule forms a HB with another O if

$$\begin{aligned} r &\le r_{HB} = 0.35\,\text{nm} \\ \alpha &\le \alpha_{HB} = 30^\circ, \end{aligned} \tag{3}$$

where r is the distance between the donor and acceptor and α is the OH–O angle.

We characterize the dynamics of water within the $AlPO_4$-54 nanopores by calculating the diffusion coefficient of water and water rotational relaxation time, τ. To determine the diffusion coefficient, we first calculate the mean square displacement, MSD, given by

$$\langle r^2(t)\rangle = \langle [r(t_0 + t) - r(t_0)]^2\rangle, \tag{4}$$

and the diffusion coefficient was computed from Einstein equation

$$D = \lim_{\tau\to\infty} \frac{1}{2d}\frac{d}{d\tau}\langle r^2(t)\rangle, \tag{5}$$

where d is the dimensionality of the system. The rotational autocorrelation function is computed from

$$C_p^n(t) = \int_0^\infty P_n(\cos(\theta_p(\xi)))d\xi, \tag{6}$$

where $P_n(x)$ is the nth order Legendre polynomial and $\theta_p(\xi)$ is the angle between $p(\xi)$ and $p(\xi + t)$. $p(\xi)$ is the orientation of the molecule at $t = \xi$. The relaxation time, τ, can be obtained by fitting the rotational autocorrelation function with

$$C = a_1\exp(-t/\tau_1) + a_2\exp(-t/\tau_2), \tag{7}$$

where a_1 and a_2 are constants and τ_1 and τ_2 are the slow and fast relaxation times, respectively.

III. RESULTS

We present our results in two separate sections. First, we discuss the structure of water within the nanopore; next, the water dynamic properties are presented.

A. Water structure

To characterize the water structure within the nanopores, the density profile, $\rho(r)$, is analyzed. Figure 2 shows $\rho(r)$ for all temperatures and water loadings studied. The maxima and minima in $\rho(r)$ indicate the formation of layers within the pores. Interestingly, we find that, even at very small water loadings, water molecules form a preferential layer near the wall at a distance of $r \approx 0.55$ nm from the center of the nanotube. This hydration layer at the nanopore surfaces is a consequence of the strong hydrophilic interactions due to the large relative charges of O, Al, and P (see Table I). At all temperatures studied, we find that increasing the water content within the pores leads to the formation of a second layer at $r \approx 0.4$ nm and a third layer at $r \approx 0.15$ nm. Considering that the distance between the two oxygen atoms in a hydrogen bond is $d \approx 0.28$ nm, we could expect that the second and third layers of the water would be separated from each other by a

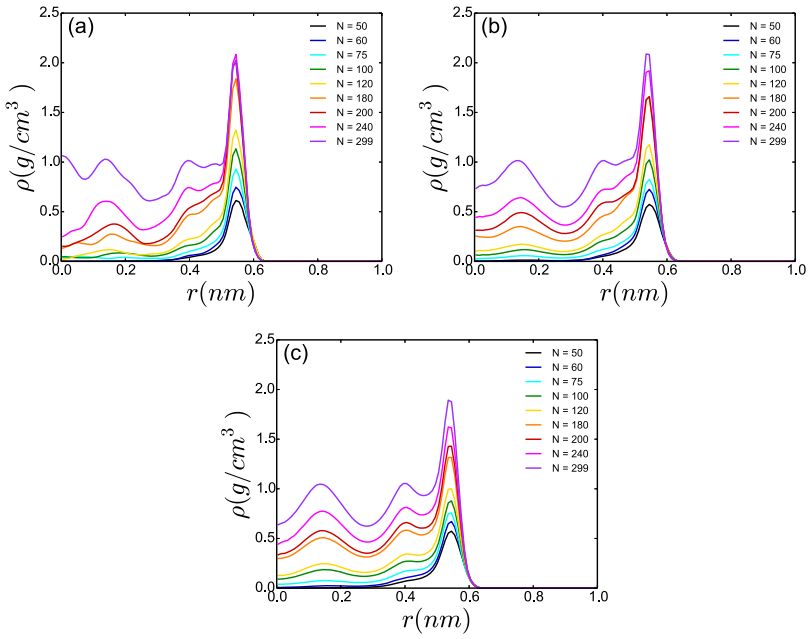

FIG. 2. Density profile for (a) $T = 173$ K, (b) $T = 235$ K, and (c) $T = 293$ K and all the values of water loading studied. The distance r is measured from the center of the nanotube.

distance of 0.3 nm, what allows for the formation of undistorted hydrogen bonds. Instead, we observe that the distance between the second and first layers of water is rather small, 0.1 nm, and hence the water molecules in the second and third layers are closer than 0.3 nm and form only, if any, highly distorted H-bonds. It follows that the interactions of water with the nanopore surface and the small pore radius affect considerably the structure of water in the second and third hydration layers.

Figure 2 also shows that as the water loading is increased, the density of the contact layer also steadily increases with the exception of the system at temperature T = 173 K for which the contact layer is possibly already frozen in its maximum density at water loadings n = 180 or higher.

Figure 3 shows the planar density as colormaps, $\rho(x, y)$, for low (N = 50), medium (N = 180), and high (N = 299) loadings and for all temperatures studied. The red regions represent the higher probability of finding a water molecule while the dark blues are the regions with the lower probability. The density colormaps illustrate that at low densities the water molecules are located only near the pore wall notwithstanding the temperature, as already suggested by Fig. 2. Interestingly, the distribution of water molecules over the inner pore surface is not uniform, but it is concentrated in certain positions of the wall. As the number of molecules is increased, the second and third layers are formed, but the water distribution within the pore and at the interface remains highly heterogeneous. The water molecules close to the wall might be located at regions in which water-wall HBs are present.

In order to identify the regions of the wall which are more attractive to the water molecules, we show the density maps $\rho(z, \theta)$. $\rho(z, \theta)$ quantifies the local density of water in the first hydration layer as a function of the pore height z and polar angle θ. By comparing $\rho(z, \theta)$ with the location of Al, P, and O at the pore inner surface, we can identify the sites of the pore surface that are the most or the least attractive to water molecules. The Al and O atoms of the $AlPO_4$-54 matrix and

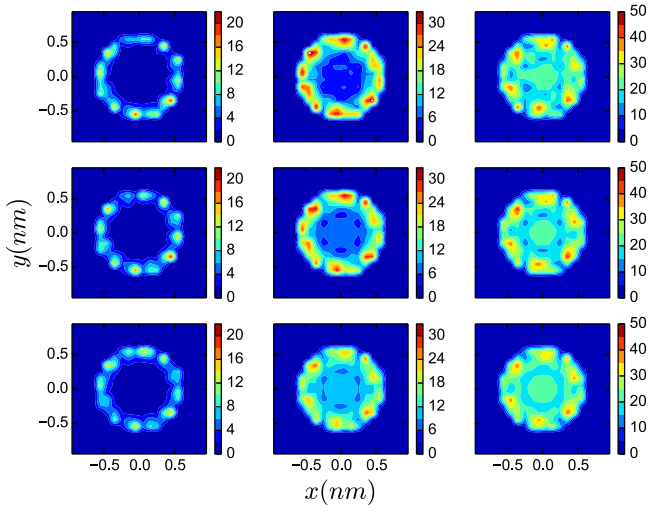

FIG. 3. x-y colormaps for T = 173 K (first line), T = 235 K (second line), and T = 293 K (third line) and N = 50 (first column), N = 180 (second column), and N = 299 (third column). The red regions represent the higher probability of finding a water molecule, while the dark blues are the regions with the lower probability.

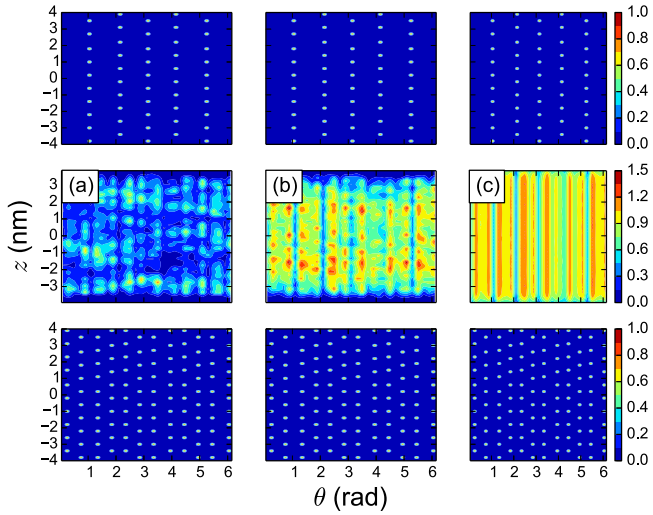

FIG. 4. $\theta - z$ colormaps for (a) N = 50, (b) N = 180, and (c) N = 299 for T = 293 K. The top graphs represent the position of the aluminum atoms, and the bottom graphs represent the position of the oxygen atoms at the $AlPO_4$-54 matrix. The red regions represent the higher probability of finding a water molecule, while the dark blues are the regions with the lower probability.

the water at the contact layer are shown as a planar surface and θ-z colormaps were used. Figure 4 illustrates these colormaps for T = 293 K and N = 50, 180, and 299 (middle row). The top and bottom rows of Fig. 4 indicate the location of the aluminum and the oxygen atoms of the nanopores' inner surface, respectively. The red (blue) regions represent the high (low) probability of finding a water molecule near the nanopore wall. The main point of Fig. 4 is that, for all the three loadings, the water molecules correlate with the location of the O atoms of the matrix and anti-correlate with the location of the Al atoms. Such a correlation between the local density of water and the location of the O atoms in the pore becomes more pronounced with increasing the water content within the pore.

This behavior can also be seen in Fig. 5, where we show the water molecules in the first hydration layer as a function of z and θ, i.e., this is the view of the water molecules in contact with the pore as seen from the pore axis. In Fig. 5, only atoms that are in direct contact with the confined water are included, i.e., Al and O atoms. The blue and the yellow spheres represent the Al and O atoms of the pore while the red and white spheres are the O and H atoms of the water molecules, respectively.

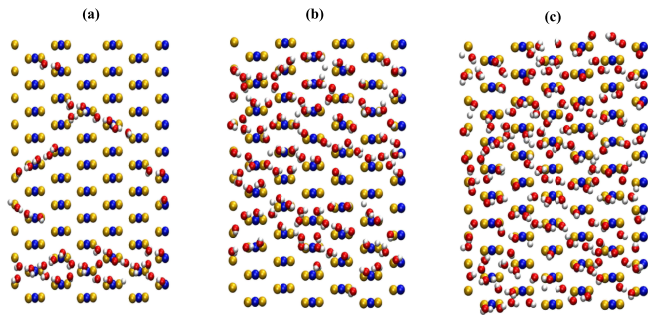

FIG. 5. $\theta - z$ snapshots of the system for (a) N = 50, (b) N = 180, and (c) N = 299 for T = 293 K. Blue spheres represent the aluminum and yellow spheres represent the oxygen belonging to $AlPO_4$-54.

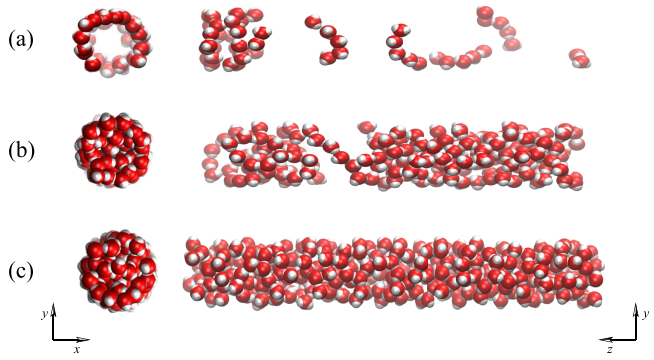

FIG. 6. Snapshots of the system for (a) $N = 50$, (b) $N = 180$, and (c) $N = 299$ for $T = 293$ K. The x-y snapshots (left) and z-y snapshots (right) are shown.

As an example, we focus on the cases $T = 293$ K and $N = 50$, 180, and 299. The snapshots clearly indicate that the water molecules in the first hydration layer tend to be closer to the O atoms than to the Al atoms of the matrix, confirming the correlation and anti-correlation observed in Fig. 4.

Remarkably, for low water loading, the location of the pore O atoms favors water molecules to arrange in string-like, helix structures. These structures can be seen in the case of $N = 50$, by the diagonal lines of water in the middle panel of Fig. 5(a) and in Fig. 6(a). The formation of such structure was also observed in experiments and other simulations.[43,44] As the water loading increases, many layers are formed within the pore and the helix structure becomes less visible; see, e.g., Figs. 6(b) and 6(c) for the cases of $N = 180$ and $N = 299$, respectively.

The preferential hydration of the O atoms in the pore inner surface can be understood in terms of the number of HBs that water molecules form with other water molecules and with the O atoms of the pore. Figure 7 shows the number of HBs per water molecule as a function of the water loading. The total number of hydrogen bonds per water molecules is close to 4, as expected for a perfect tetrahedral network, and decreases slightly with the increase of the temperature, due to entropic effects. For $N = 50$, shown in Fig. 7(a), the number of water-water and water-$AlPO_4$-54 HBs is almost the same. In order to maintain four total HBs, with O in the wall without breaking bonds with the other water molecules in the same layer, the surface water molecules form a linear helix-like structure. As the loading increases, as illustrated in Figs. 7(b) and 7(c), more layers of water are formed and the number of water-water bonds increases.

In summary, our results indicate that the confined fluid forms heterogeneous layers and that for lower water loadings, the formation of a helicoidal structure allows the water molecules to form more water-water H-bonds without distorting the structure imposed by $AlPO_4$-54.

B. Water dynamics

In order to better understand the dynamics of the system, we focus, first, on the MSD and on the diffusivity of water within the pores. The diffusion coefficient for all cases was obtained only considering the z contributions to the MSD since the Einstein relation is valid only for $t \longrightarrow \infty$. Figure 8 shows the MSD and the diffusion coefficient obtained using Eq. (5) for the case $T = 173$ K and various loadings. At this temperature, the dynamics is slow and the diffusive regime is not completely reached during the simulated time. The diffusion coefficient in this case is obtained using the few linear points in Fig. 8(c). Accordingly, the diffusion coefficients at this temperature are estimated values that set a lower boundary for water diffusion coefficients. It is remarkable that at this temperature water still exhibits translational motion within our 40 ns simulation run. For comparison, bulk water at $T = 173$ K cannot be experimentally studied in the liquid state due to unavoidable crystallization. Similarly, bulk TIP4P/2005 water cannot be equilibrated at this temperature even within 1 microsecond-simulation runs. It follows that, relative to the

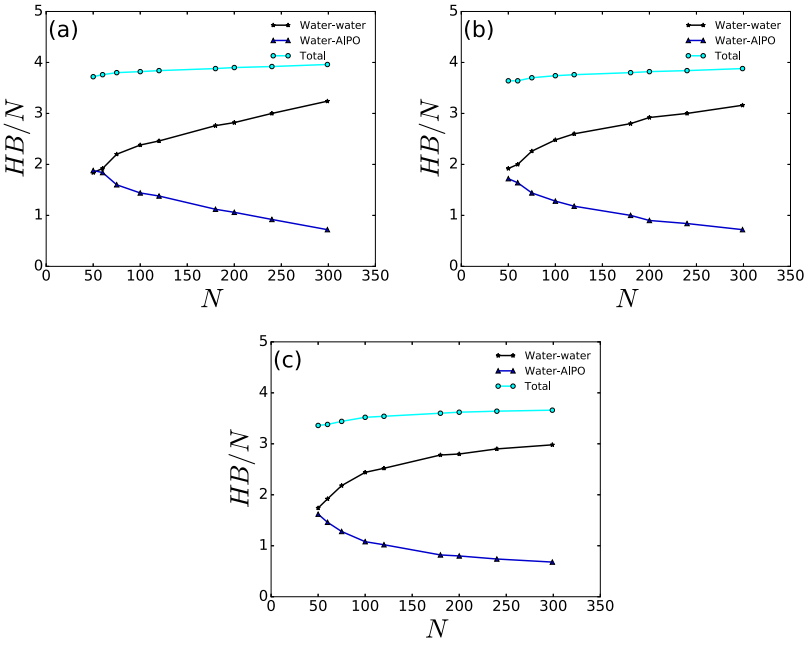

FIG. 7. Average number of HBs per water molecule as a function of the water loading for (a) $T = 173$ K, (b) $T = 235$ K, and (c) $T = 293$ K. Total number of H-bonds, water-water H-bonds, and water-$AlPO_4$-54 H-bonds are shown.

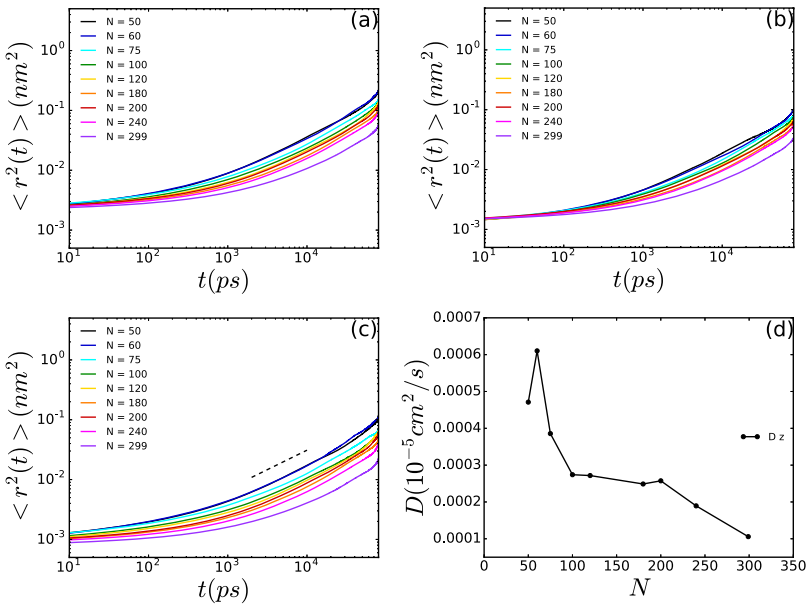

FIG. 8. Mean square displacement, $\langle r^2(t) \rangle$, (a) total, (b) on the x-y plane, (c) on the z axis, and (d) the z direction diffusion coefficient for $T = 173$ K and all water loadings studied. The dashed line in (c) is a guide to the eye.

bulk case, water confined within the $AlPO_4$-54 pores exhibits an enhanced diffusivity. However, and not surprisingly, water within the $AlPO_4$-54 pores diffuses much slower than in carbon nanotubes.[45] At $T = 173$ K, increasing the water loading within the pores leads to a decrease in the MSD and in the diffusion coefficients [Fig. 8(d)]. The decrease of the diffusion with the increase of the water loading observed for $T = 173$ K and $N > 60$ is not surprising since more space (lower N) favors mobility. For $N < 60$, however, the increase in N increases mobility. In this case, the increase of mobility is due to the change in the behavior of the HBs where the water molecules lose HBs with the wall and form with other water molecules, as shown in Fig. 7(a). This anomalous behavior for low N was also observed in simulations for water confined in MCM-41 pores.[46]

The MSD and the diffusion coefficients at $T = 235$ and 293 K are shown in Figs. 9 and 10, respectively. As expected, for a given water loading, increasing the temperature leads to an increase in the MSD and in the diffusivity. In these temperatures, contrary to the low temperature behavior, increasing the water content in the pores enhances the diffusivity of water. The increase in the mobility with water loadings is also observed in bulk water in the diffusion anomalous region. The mechanism is not due to the change in the number of HBs but the increase of the number of neighbors leading to the formation of interstitial water and distorted bonds. At very high water loadings, the water molecules have their mobility suppressed on the x-y plane by the confining environment. The suppression is shown in Figs. 9(b) and 10(b) as a plateau on the MSD.

Next, we focus on the rotational dynamics of the system, and we calculate the rotational autocorrelation function of the water molecules within the pore. The orientational relaxation time is calculated from these functions using the following

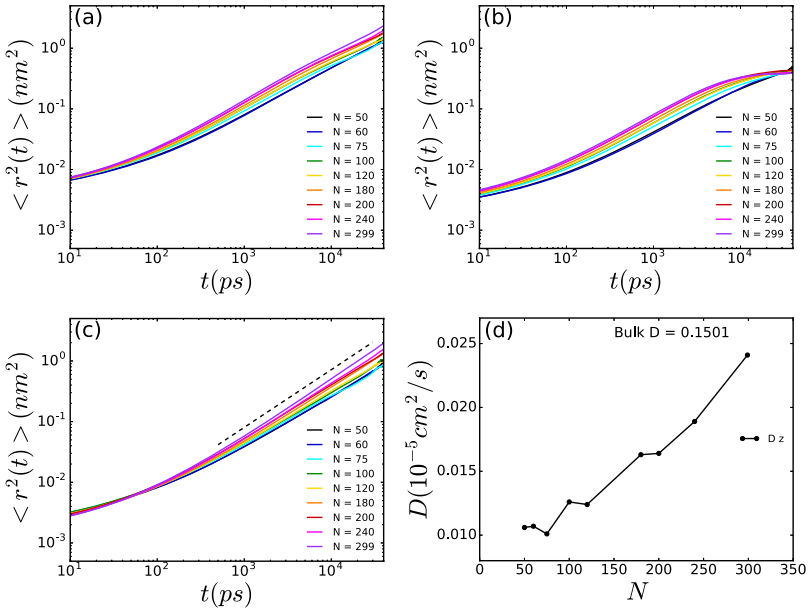

FIG. 9. Mean square displacement, $\langle r^2(t) \rangle$, (a) total, (b) on the x-y plane, (c) on the z axis, and (d) the z direction diffusion coefficient for $T = 235$ K and all water loadings studied. The upper D value in (d) indicates the simulated diffusion of bulk water at $T = 235$ K and $\rho = 0.98$ g/cm^3. The dashed line in (c) is a guide to the eye.

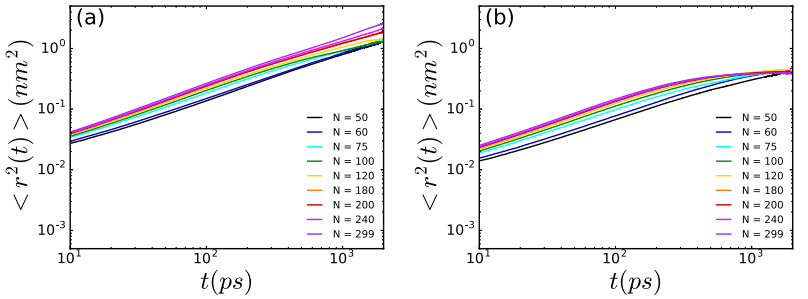

FIG. 10. Mean square displacement, $\langle r^2(t) \rangle$, (a) total, (b) on the x-y plane, (c) on the z axis, and (d) the z direction diffusion coefficient for $T = 293$ K and all water loadings studied. The upper D value in (d) indicates the simulated diffusion of bulk water at $T = 293$ K and $\rho = 0.98$ g/cm^3. The dashed line in (c) is a guide to the eye.

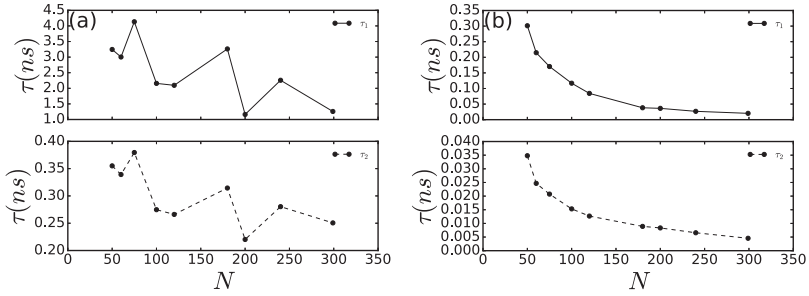

FIG. 11. Relaxation times as a function of the water loading for (a) $T = 235$ K and (b) $T = 293$ K. Solid lines represent the relaxation time for the slow reorientation process and the dashed line represents the relaxation time for the fast reorientation process.

fitting function:

$$C = a_1 \exp(-t/\tau_1) + a_2 \exp(-t/\tau_2). \quad (8)$$

In most cases, only one relaxation time is needed for a good fit; however, in our case two relaxation times, τ_1 and τ_2, were used in order to take into account the possibility of having a fast and a slow reorientation process. The non-exponential dynamics of confined water is due to the broad distribution of the H-bond partners' exchange rate induced by the heterogeneity of the pore surface.[47] Figure 11 shows these relaxation times as a function of the water loading for $T = 235$ K and $T = 293$ K. A table with the values of a_1 and a_2 for all the water loadings and temperatures studied can be found in the supplementary material.

For $T = 173$ K (not shown), a very slow dynamics is observed with relaxation time, for the slow reorientation process, even larger than the simulated time. With the increase of the temperature, the relaxation time decreases, and the same trend is observed for the slow and the fast reorientation processes for $T = 235$ K and $T = 293$ K (Fig. 11), respectively: With the increase of the water loading, the relaxation time decreases. Therefore, the rotational dynamics for higher temperatures follows the same trend as the translational dynamics [Figs. 9(c) and 10(d)]: the mobility increases with the increase of the water loading, which is the same mechanism of the diffusion anomaly in bulk water. The formation of the helix structure for low values of N leads to stronger HB, which hinders the reorientational process. As N increases and the helix structure disappears, it became easier for the water molecules to exchange HBs and, as a result, the reorientational processes are faster.

Thus, the analysis of the MSD, diffusion coefficient, and angular correlation function indicates that the water confined in $AlPO_4$-54 nanotubes does not crystallize even at $T = 173$ K, and its dynamics is enhanced within the pore relative to the bulk. In addition, water's dynamics is enhanced by increasing T and the water loading within the pore.

IV. CONCLUSION

In the present work, we studied the structure and the mobility of water confined inside the $AlPO_4$-54 nanotube through molecular dynamics simulations in order to identify if it crystallizes for similar temperatures as observed in the bulk or if it remains liquid or glassy. Simulations were performed for $T = 173$ K, $T = 235$ K, and $T = 293$ K and water loadings of $N = 50$, 60, 75, 100, 120, 180, 200, 240, and 299.

We observed, for all cases, that the water confined in $AlPO_4$-54 also forms layers similarly to what was observed for other confined systems[17–22] and that these layers are not uniformly distributed. In the particular case of $AlPO_4$-54, the water molecules are located near O of the confining matrix, forming empty regions close to Al. In order to maintain the H-bonds with the oxygens of $AlPO_4$-54 and with the other water molecules, the system forms a mobile helix at low loadings for all temperatures.

For T = 173 K, an enhancement in the diffusion coefficient when compared with the bulk is observed; however, the diffusion coefficient and the relaxation times obtained lead to the conclusion that the system has a very slow dynamics indicating that the confined water could be in a glassy state. This result is compatible with the previous work from Alabarse *et al.*;[34] however, it is not clear if the system is all in one phase or if the water exhibits a multiphase structure as observed in other confined systems.[48] For very low water loadings, the presence of the structured helix formation may indicate the beginning of crystallization.

For higher temperatures, T = 235 K and T = 293 K, no frozen state is observed confirming that the melt of the confined water in $AlPO_4$-54 occurs for temperatures much below the bulk value.[34] Anomalous diffusivity behavior where D increases with the increase of N is observed in this case. This occurs due to the increase of the number of neighbors leading to the formation of interstitial water and distorted H-bonds. The formation of a single file structure in the form of a helix, in this case, might be interesting in the study of the single file superflow used in desalination processes.

SUPPLEMENTARY MATERIAL

See supplementary material for additional results.

ACKNOWLEDGMENTS

We thank the Brazilian agency CNPq for the financial support.

[1] S. T. Wilson, B. M. Lok, C. A. Messina, T. R. Cannan, and E. M. Flanigen, J. Am. Chem. Soc. **104**, 1146 (1982).
[2] W. M. Meier and D. H. Olson, Zeolites **12**, 1 (1992).
[3] F. G. Alabarse, J.-B. Brubach, P. Roy, A. Haidoux, C. Levelut, J.-L. Bantignies, O. Cambon, and J. Haines, J. Phys. Chem. C **119**, 7771 (2015).
[4] J. W. Richardson, Jr., J. V. Smith, and J. J. Pluth, J. Phys. Chem. **93**, 8212 (1989).
[5] G. Hummer, J. C. Rasaiah, and J. P. Noworyta, Nature **414**, 188 (2001).
[6] M. M. Majunder, N. Chopra, R. Andrew, and B. J. Hinds, Nature **438**, 44 (2005).
[7] J. K. Holt, H. G. Park, Y. Wang, M. Stadermann, A. B. Artyukhin, C. P. Grigoropoulos, A. Noy, and O. Bakajin, Science **312**, 1034 (2006).
[8] X. Q. Qin, Q. Yuan, Y. Zhao, S. Xie, and Z. Liu, Nano Lett. **11**, 2173 (2010).
[9] S. Wang and Y. Peng, Chem. Eng. J. **156**, 11 (2010).
[10] S. Babel and T. A. Kurniawan, J. Hazard. Mater. **97**, 219 (2003).
[11] L. B. Krott and M. C. Barbosa, Phys. Rev. E **89**, 012110 (2014).
[12] J. R. Bordin, L. B. Krott, and M. C. Barbosa, J. Phys. Chem. C **118**, 9497 (2014).
[13] Z. W. Ulissi, S. Shimizu, C. Y. Lee, and M. S. Strano, J. Phys. Chem. Lett. **2**, 2892 (2011).
[14] F. Fornasiero, H. G. Park, J. K. Holt, M. Stadermann, C. P. Grigoropoulos, A. Noy, and O. B. Bakajin, Proc. Natl. Acad. Sci. U. S. A. **105**, 17250 (2005).
[15] K. P. Lee, H. Leese, and M. Mattia, Nanoscale **4**, 2621 (2012).
[16] M. Heiranian, A. B. Farimani, and N. R. Aluru, Nat. Commun. **6**, 8616 (2015).
[17] R. Zangi and A. E. Mark, J. Chem. Phys. **119**, 1694 (2003).
[18] L. Krott, J. R. Bordin, N. M. Barraz, and M. C. Barbosa, J. Chem. Phys. **142**, 134502 (2015).
[19] M. H. Köhler and L. B. da Silva, Chem. Phys. Lett. **645**, 38 (2016).
[20] P. Gallo, M. Rapinesi, and M. Rovere, J. Chem. Phys. **117**, 369 (2002).
[21] P. Gallo, M. Rovere, and S. Chen, J. Phys.: Condens. Matter **24**, 064109 (2012).
[22] P. Gallo, M. Rovere, and S.-H. Chen, J. Phys. Chem. Lett. **1**, 729 (2010).
[23] T. Nanok, N. Artrith, P. Pantu, P. A. Bopp, and J. Limtrakul, J. Phys. Chem. A **113**, 2103 (2008).
[24] K. Morishige and K. Kawano, J. Chem. Phys. **110**, 4867 (1999).
[25] N. Giovambattista, P. J. Rossky, and P. G. Debenedetti, J. Phys. Chem. B **113**, 13723 (2009).
[26] N. Giovambattista, P. J. Rossky, and P. G. Debenedetti, Phys. Rev. E **73**, 041604 (2006).
[27] K. Koga, X. C. Zeng, and H. Tanaka, Phys. Rev. Lett. **79**, 5262 (1997).
[28] P. Kumar, S. V. Buldyrev, F. W. Starr, N. Giovambattista, and H. E. Stanley, Phys. Rev. E **72**, 051503 (2005).
[29] E. B. Moore, J. T. Allen, and V. Molinero, J. Phys. Chem. **116**, 7507 (2012).
[30] K. Koga, G. T. Gao, H. Tanaka, and X. C. Zeng, Nature **412**, 802 (2001).
[31] V. Sánchez-Gil, E. G. Noya, J. M. Guil, E. Lomba, and S. Valencia, Microporous Mesoporous Mater. **222**, 218 (2016).
[32] G. H. Findenegg, S. Jähnert, D. Akcakayiran, and A. Schreiber, ChemPhysChem **9**, 2651 (2008).
[33] S. Jähnert, F. V. Chávez, G. E. Schaumann, A. Schreiber, M. Schönhoff, and G. H. Findenegg, Phys. Chem. Chem. Phys. **10**, 6039 (2008).
[34] F. G. Alabarse, J. Haines, O. Cambon, C. Levelu, D. Bourgogne, A. Haidoux, D. Granier, and B. Coasne, Phys. Rev. Lett. **109**, 035701 (2012).
[35] J. L. F. Abascal and C. Vega, J. Chem. Phys. **123**, 234505 (2005).
[36] C. Vega and J. L. F. Abascal, Phys. Chem. Chem. Phys. **13**, 19663 (2011).
[37] C. A. Koh, T. Montanari, R. I. Noomey, S. F. Tahir, and R. E. Westacott, Langmuir **15**, 6043 (1999).
[38] H. J. Berendsen, D. van der Spoel, and R. van Drunen, Comput. Phys. Commun. **91**, 43 (1995).
[39] E. Lindahl, B. Hess, and D. Van Der Spoel, Mol. Model. Annu. **7**, 306 (2001).
[40] D. Van Der Spoel, E. Lindahl, B. Hess, G. Groenhof, A. E. Mark, and H. J. Berendsen, J. Comput. Chem. **26**, 1701 (2005).
[41] S. Nosé, Mol. Phys. **52**, 255 (1984).
[42] B. Hess, H. Bekker, H. J. Berendsen, J. G. Fraaije *et al.*, J. Comput. Chem. **18**, 1463 (1997).
[43] P. Demontis, J. Gulín-González, M. Masia, and G. B. Suffritti, J. Phys.: Condens. Matter **22**, 284106 (2010).
[44] P. Demontis, J. Gulín-González, and G. B. Suffritti, J. Phys. Chem. C **116**, 11100 (2012).
[45] Y.-G. Zheng, H.-F. Ye, Z.-Q. Zhang, and H.-W. Zhang, Phys. Chem. Chem. Phys. **14**, 964 (2012).
[46] P. Gallo, M. Rovere, and S. Chen, J. Phys.: Condens. Matter **22**, 284102 (2010).
[47] A. C. Fogarty, E. Duboué-Dijon, D. Laage, and W. H. Thompson, J. Chem. Phys. **141**, 18C523 (2014).
[48] A. Barati Farimani and N. R. Aluru, J. Phys. Chem. C **120**, 23763 (2016).